Wave propagation and growth on a surface front in a two-layer geostrophic current

Article *in* Journal of Marine Research · November 1984

DOI: 10.1357/002224084788520701

CITATIONS
101

READS
49

3 authors, including:

Nathan Paldor
Hebrew University of Jerusalem
138 PUBLICATIONS **1,525** CITATIONS

SEE PROFILE

Journal of Marine Research, 42, 761–785, 1984

Journal of
MARINE RESEARCH

Volume 42, Number 4

Wave propagation and growth on a surface front in a two-layer geostrophic current

by Peter D. Killworth,[1] Nathan Paldor[2] and Melvin E. Stern[3]

ABSTRACT

We study analytically and numerically small amplitude perturbations of a geostrophically balanced semi-infinite layer of light water having a surface front and lying above a heavier layer of *finite* vertical thickness which is at rest in the mean. In contrast with previous studies where the latter layer was infinitely deep we find that the equilibrium is always unstable regardless of the distribution of potential vorticity, and the maximum growth rates are generally much larger than in the "one-layer" case. The amplifying ageostrophic wave transfers kinetic energy from the basic shear flow as well as potential energy. Good quantitative agreement is found with the laboratory experiments of Griffiths and Linden (1982), and our model seems to be the simplest one for future investigations of cross frontal mixing processes by finite amplitude waves. The propagation speed of very low frequency and nondispersive frontal waves is also computed and is shown to decrease with increasing bottom layer depth.

1. Introduction

Fronts are frequent synoptic features of both the atmosphere and the ocean (Hoskins, 1982; Legeckis, 1978). They are important in the ocean because they are believed to be the site of much of the oceanic dissipation and mixing (Joyce, 1980). This is in part because the flow at fronts is known to be highly unstable; both observationally, e.g. the Gulf Stream (Fofonoff, 1981), and in the laboratory (Griffiths and Linden, 1982; Chia *et al.*, 1982). Our previous frontal studies have been largely

1. Department of Applied Mathematics and Theoretical Physics, University of Cambridge, Silver Street, Cambridge, England.
2. Department of Isotope Research, Weizmann Institute of Science, Rehovot 76100, Israel.
3. Graduate School of Oceanography, University of Rhode Island, Kingston, Rhode Island, 02881, U.S.A.

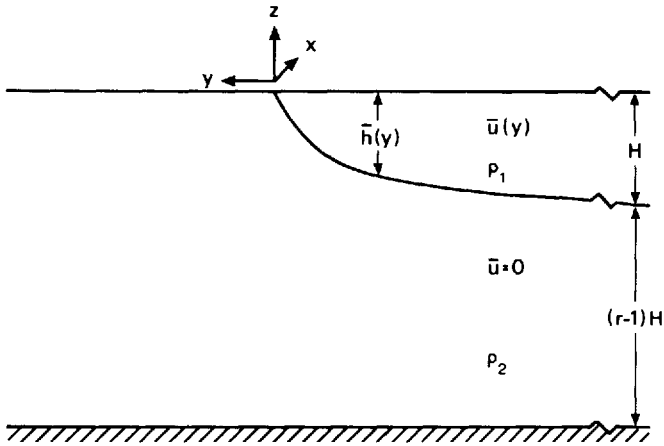

Figure 1. The frontal configuration used in this paper.

motivated by a desire to understand these latter laboratory studies, but hitherto the theory has been restricted to only one active layer of fluid. This omitted at least one fundamental mode of instability such as happens in the classical Phillips (1954) model for nonfrontal configurations. The frontal model to be considered here (Fig. 1) differs from its predecessors because it has *two* active layers of fluid which are actively coupled.

In the one layer study of Griffiths *et al.* (1981), hereafter GKS, a density current having two fronts on the same level surface was studied theoretically and experimentally and shown to be highly unstable when the distance between these two fronts was not large compared to the Rossby radius of deformation. Otherwise substantial disagreement between theory and experiment was found, and this was attributed to the presence of another kind of instability mode. Paldor (1983) showed that a single-layer front (semi-finite) with uniform potential vorticity was completely stable and the dispersion relation for the frontal waves was computed. Killworth (1983) showed that this front is destabilized if the layer tends to uniform depth at infinity more rapidly than a layer of constant potential vorticity of the same depth. The effect of a vertical boundary, which is relevant to coastal fronts, was examined by Killworth and Stern (1982), hereafter KS, who showed that the potential vorticity (evaluated at the boundary) must be increasing toward the vertical boundary in order for instability to occur. Reference should also be made to preliminary attempts (Stern *et al.*, 1982) to investigate finite amplitude frontal waves by means of a long-wave approximation to the shallow water equations. In summary, none of these one-layer theories seem to furnish an acceptable starting point for explaining the interesting observations of Griffiths and Linden (1982).

It will come as no surprise, with quasi-geostrophic theory as a well-known precedent (Pedlosky, 1979) that a new and important ingredient will appear in the frontal

dynamics when the two layers (Fig. 1) have comparable vertical thickness. On the other hand, we must emphasize the inapplicability of quasi-geostrophic theory to the problem at hand. It is not only a question of exceeding the formal limits of validity (on the Rossby number and on the variability of layer thickness). The central question is the prediction of the lateral displacement of the front up to the (highly nonlinear) point where cross-frontal mixing occurs via eddies which detach from their parent water mass and cross over to the other side of the front. It seems to us that the nearest thing to an acceptable frontal model is that of Orlanski (1968), but that has a bottom front and a surface front.

We therefore propose to generalize the earlier work on a single front (Fig. 1) by considering the effect of finite total depth on the growth of small amplitude frontal perturbations. A proper asymptotic expansion (in downstream wave number) of the ageostrophic shallow water equations will show (Sections 4 and 5) that the equilibrium in Figure 1 is unstable, regardless of the distribution of potential vorticity in the upper layer. The most fundamental (and simplest) case of uniform potential vorticity is then examined in detail by a numerical calculation for a range of wave numbers and for various r. The wavelength of the fastest growing mode is compared to the Griffiths and Linden experiment and is in excellent agreement. We also compute the ratio of the release of kinetic energy to the release of potential energy, a number which may be accessible in oceanic measurements of frontal currents (Lee and Atkinson, 1983).

Although this baroclinic instability mode is the fastest growing and must be important for the synoptic scale, there is another mode (Section 3) which is nondispersive at low frequencies, and which is of interest in connection with the annual variation of the Loop Current in the Gulf of Mexico.

2. Formulation of the problem

Figure 1 is a vertical section through a geostrophic flow of a light fluid layer (density ρ_1) which overrides a layer of heavier fluid (density $\rho_2 > \rho_1$). (This shows the oceanic configuration; for atmospheric problems, invert the vertical axis and density ratio.) The interface between the two layers intersects the surface at $y = y_f(x, t)$, and its depth approaches a constant dimensional value H as $y \to -\infty$. The thickness of the *lower* layer at $y \to -\infty$ is taken to be $(r-1)H$. The shallow water equations for each of the layers are nondimensionalized by scaling the cross-stream coordinate (y) by the radius of deformation $R = (g(\rho_2 - \rho_1)H\rho_2^{-1})^{1/2}/f$ and the downstream coordinate by $\epsilon^{-1}R$, $\epsilon \ll 1$. (Analytically, ϵ will be small. Numerically, no such limit is made.) This scaling anticipates that attention will be directed to the long wave limit $\epsilon \to 0$, where ϵ will play the role of a downstream wavenumber. The time (t) is accordingly scaled by $(\epsilon f)^{-1}$, the downstream velocity (u) is scaled by $V = (g(\rho_2 - \rho_1)\rho_2^{-1}H)^{1/2}$, and the smaller cross-stream velocity is scaled by ϵV. The depth of the interface (h) is scaled by H, so that the nondimensional value of the depth of the interface at $y = -\infty$ is 1, while the lower layer thickness at $-\infty$ is $(r-1)$. Letting $\zeta = \epsilon^2 v_x - u_y$ denote the relative

vorticity and p the pressure (nondimensionalized by $g(\rho_2 - \rho_1)H^{-1}$), the horizontal momentum equations for either layer are:

$$\frac{\partial u_i}{\partial t} - (1 + \zeta_i)v_i = \frac{\partial}{\partial x}\left(p_i + \frac{u_i^2}{2} + \epsilon^2 \frac{v_i^2}{2}\right) \tag{2.1}$$

$$\epsilon^2 \frac{\partial v_i}{\partial t} + (1 + \zeta_i)u_i = \frac{-\partial}{\partial y}\left(p_i + \frac{u_i^2}{2} + \epsilon^2 \frac{v_i^2}{2}\right), \tag{2.2}$$

where $i = 1,2$ represents upper, lower layer respectively. Henceforth the upper layer pressure will be denoted by ϕ, the lower by p, to simplify notation. The continuity equation in the upper layer is

$$\frac{\partial h}{\partial t} + \frac{\partial}{\partial x}(u_1 h) + \frac{\partial}{\partial y}(v_1 h) = 0, \tag{2.3}$$

while in the lower layer this equation becomes

$$\frac{\partial}{\partial t}(r - h) + \frac{\partial}{\partial x}(u_2(r - h)) + \frac{\partial}{\partial y}(v_2(r - h)) = 0. \tag{2.4}$$

The hydrostatic relation between the pressure in the upper and lower layers can be written as:

$$\nabla h(x, y, t) = \nabla(\phi - p). \tag{2.5}$$

We recall that (2.1) to (2.4) imply the conservation in each layer of the potential vorticity:

$$Q_1 \equiv \frac{\zeta_1 + 1}{h} \tag{2.6}$$

$$Q_2 \equiv \frac{\zeta_2 + 1}{r - h} \tag{2.7}$$

so that

$$\left(\frac{\partial}{\partial t} + u_i \frac{\partial}{\partial x} + v_i \frac{\partial}{\partial y}\right) Q_i = 0, \qquad i = 1,2. \tag{2.8}$$

We consider henceforth small perturbations to a mean state (the latter is denoted by bars) in which there is no mean flow in the lower layer, and the upper layer is in geostrophic balance. We choose a steady mean zonal geostrophic flow $\bar{u}(y)$ in the upper layer so that

$$\bar{u}_1 \equiv \bar{u} = -\bar{h}_y, \bar{\phi} = \bar{h}(y), \bar{p} = 0, \bar{u}_2 = \bar{v}_2 = \bar{v}_1 = 0.* \tag{2.9}$$

*The necessity for geostrophy comes from (2.2); the choice of zero for $\bar{p}$ is arbitrary as this has no effect on the dynamics.

The function $\bar{h}(y)$ is chosen so as to tend to unity as $y \to -\infty$, and $\bar{h}$ vanishes at $y = 0$, so that the mean front y_f occurs at the origin. For $y > 0$, there is only lower layer fluid, at rest in the mean state.

For the special case of uniform potential vorticity in the upper layer (Q_1 is a constant, and the condition at infinity implies $Q_1 = 1$), $\bar{h}$ and $\bar{u}$ satisfy

$$\bar{h} = 1 - e^y \tag{2.10}$$

$$\bar{u} = e^y \tag{2.11}$$

as seen from (2.6) and (2.9), together with $\bar{h}(0) = 0$.

We now assume the (x, t) structure of the small perturbations to be that of a *normal mode*, here $\exp i(x - ct)$. The parameter ϵ, as noted, plays the role of a wavenumber, and because of the scaling already performed does not appear in the exponential. Nonetheless, the unknown phase velocity c still carries the usual connotations: real c implies stability, while complex c, with $Im(c)$ positive, implies instability. In the latter case, $\epsilon\, Im(c)$ is the growth rate.

The linear perturbations then satisfy

$$(\bar{u} - c)u_1 + (1 - \bar{u}_y)iv_1 + \phi = 0 \tag{2.12}$$

$$\epsilon^2(\bar{u} - c)iv_1 + u_1 + \phi_y = 0 \tag{2.13}$$

$$\bar{h}u_1 - (\bar{h}iv_1)_y + (\bar{u} - c)h = 0 \tag{2.14}$$

$$-cu_2 + iv_2 + p = 0 \tag{2.15}$$

$$-\epsilon^2 civ_2 + u_2 + p_y = 0 \tag{2.16}$$

$$-(r - \bar{h})u_2 + ((r - \bar{h})iv_2)_y - ch = 0. \tag{2.17}$$

The lower-layer equations (2.15) to (2.17) may be combined to obtain a single equation for p and h, by solving for u_2, v_2 from (2.15), (2.16). Upon substituting in (2.17) we obtain

$$c[(r - \bar{h})p_y]_y = c(\epsilon^2 c^2 - 1)h + \epsilon^2 c(r - h)p - \bar{u}p. \tag{2.18}$$

For the upper-layer equations we now drop the subscript on u_1, and set $v_1 = -iV$, thereby obtaining

$$(\bar{u} - c)u + (1 - \bar{u}_y)V + \phi = 0 \tag{2.19}$$

$$\epsilon^2(\bar{u} - c)V + u + \phi_y = 0 \tag{2.20}$$

$$\bar{h}u - (\bar{h}V)_y + (\bar{u} - c)h = 0. \tag{2.21}$$

Eqs. (2.18) to (2.21) need boundary conditions, and we first consider the region $y >$

y_f, where there is only heavy fluid for which $\bar{u} = 0 = \bar{h} = h$. Eq. (2.18) reduces to

$$p_{yy} = \epsilon^2 p, \text{ so that } p = p_0 \exp(-\epsilon y), \tag{2.22}$$

and we use this solution to determine a lower-layer boundary condition at the front $y = 0$. Since p_y (as well as p) must be continuous across $y = 0$ in the lower layer, we get

$$\frac{dp(0)}{dy} + \epsilon p(0) = 0, \tag{2.23}$$

as the frontal boundary condition for the bottom pressure in the region $y \leq 0$. At large distances from the fronts in the light fluid, the boundary condition is

$$p(-\infty) = \phi(-\infty) = 0 \tag{2.24}$$

and at the front we require that the solution to Eqs. (2.19) to (2.21) be well behaved near $y = 0$. If $Q_1(0)$ is finite for the mean state, then $1 - \bar{u}_y(0) = 0$ and this combined with (2.19) yields

$$(\bar{u}(0) - c)u = -\phi, y = 0. \tag{2.25}$$

From (2.20) we get

$$u = -\phi_y - \epsilon^2(\bar{u} - c)V, y = 0$$

so that (2.25) becomes, whether or not the upper layer potential vorticity is finite,

$$(\bar{u}(0) - c)\,\phi_y(0) = \phi(0) - \epsilon^2(\bar{u}(0) - c)^2 V, y = 0. \tag{2.26}$$

3. The longwave limit for flow with nearly uniform potential vorticity

In this section we examine the simple longwave limit ($\epsilon = 0$) for $Q_1 = 1$, show that only real values of c exist, and compute them as a function of r. As mentioned in Section 1, a different (and more important) mode with a more complicated $\epsilon \to 0$ limit will be considered later. We shall also consider herein small variations from $Q_1 = 1$, and find the necessary condition on Q_{1y} in order that $Im(c)$ be positive (instability). Thus we now set $\epsilon^2 = 0$ to get the upper-layer equations

$$(\bar{u} - c)u + (1 - \bar{u}_y)V + \phi = 0 \tag{3.1}$$

$$u = -\phi_y \tag{3.2}$$

$$\bar{h}u - (\bar{h}V)_y + (\bar{u} - c)h = 0 \tag{3.3}$$

and the lower-layer equation (2.18) becomes

$$[(r - \bar{h})p_y]_y + h + \frac{\bar{u}}{c}p = 0$$

or

$$[(r - \bar{h})p_y]_y + \left(1 - \frac{\bar{u}}{c}\right)p = -\phi. \tag{3.4}$$

The basic state potential vorticity in the upper layer is written following (2.6) as

$$\frac{1 - \bar{u}_y}{\bar{h}} = Q_1(y) \tag{3.5}$$

and we will focus on the limit $Q_1(y) \approx 1$.

The boundary conditions (2.22), (2.23), (2.24) and (2.26) become for $\epsilon = 0$

$$\frac{dp(0)}{dy} = 0; \qquad p(-\infty) = 0 \tag{3.6a,b}$$

$$\frac{d\phi(0)}{dy} = \frac{\phi(0)}{\bar{u}(0) - c}; \qquad \phi(-\infty) = 0. \tag{3.7a,b}$$

The long-wave perturbation potential vorticity equation corresponding to (3.1) to (3.3) may be derived from (2.19) to (2.21) as

$$-\frac{du}{dy} - hQ_1(y) = \frac{V\bar{h}dQ_1/dy}{\bar{u} - c}$$

as this may be written as

$$\frac{d^2\phi}{dy^2} - \phi = -p + S_1 + S_0 \tag{3.8}$$

where

$$S_1 \equiv (Q_1(y) - 1)(\phi - p)$$

$$S_1 \equiv \frac{V\bar{h}dQ_1/dy}{\bar{u} - c}.$$

For subsequent work in solving (3.4), (3.8), it is helpful at this point to transform the independent coordinate y into $z = e^y$, thereby mapping the $y = (-\infty, 0)$ infinite domain onto the $z = (0, 1)$ finite interval. In terms of z, Eqs. (3.4), (3.8) and the boundary conditions (3.6a,b), (3.7a,b) become

$$z\frac{d}{dz}\left(z(r - \bar{h})\frac{dp}{dz}\right) - \left(1 - \frac{\bar{u}}{c}\right)p = -\phi \tag{3.9}$$

$$z\frac{d}{dz}\left(z\frac{d\phi}{dz}\right) - \phi = -p + S_1 + S_0 \tag{3.10}$$

$$\frac{dp(1)}{dz} = 0; \quad p(0) = 0 \tag{3.11a,b}$$

$$\frac{d\phi(1)}{dz} = \frac{\phi(1)}{\bar{u}(1) - c}; \quad \phi(0) = 0 \tag{3.12a,b}$$

where

$$S_1 = (Q_1(z) - 1)(\phi - p)$$
$$S_0 = \frac{Vz\bar{h}dQ_1/dz}{\bar{u} - c}.$$

We now divide (3.9) and (3.10) by z and multiply them by p^*, ϕ^* (the complex conjugates of p, ϕ) respectively. By integrating the resulting equations between $z = 0$ and $z = 1$ using the boundary conditions (3.11a,b), (3.12a,b), adding the equations, and taking the imaginary part, we get

$$c_i\left\{\frac{|\phi(1)|^2}{|1 - c|^2} - \frac{1}{|c|^2}\int_0^1 |p|^2 dz\right\} = Im\int_0^1 \frac{\phi^*(S_1 + S_0)}{z} dz. \tag{3.13}$$

Consider first the implications when

$$Q_1 = 1, S_1 = S_0 = 0, \bar{u} = z, \bar{h} = 1 - z.$$

The general solution of (3.10) when $S_1 = 0 = S_0$ can readily be obtained by the method of Green's function, and the regular solution is

$$\phi = zA + \frac{1}{2z}\int_0^z p(z_1)z_1^2 dz_1 - \frac{z}{2}\int_0^z p(z_1)dz_1$$

where the constant A as determined from (3.12a) is

$$A = \frac{1 - c}{c}\int_0^1 pdz - \frac{1}{2}\int_0^1 (z^2 - 1)pdz.$$

Then

$$\phi(1) = \frac{1 - c}{c}\int_0^1 p(z)dz \tag{3.14}$$

and substitution of this into (3.13) yields

$$\frac{c_i}{|c|^2}\left\{\left|\int_0^1 p(z)dz\right|^2 - \int_0^1 |p(z)|^2 dz\right\} = 0, \quad (Q_1 \equiv 1). \tag{3.15}$$

By Schwartz's inequality the term in the brackets on the left-hand side of (3.15) is negative for all nontrivial $p \neq$ constant, and therefore we have proved that when $Q_1 =$

1 the only possible eigenvalues are those for which $c_i = 0$. This stability result applies to all r but not all wavenumbers, whereas Paldor (1983) has shown that all wavenumbers are stable when $r^{-1} = 0$.

We now briefly consider the case where $Q_1 - 1$ and c_i are small. Since there exist (see below) real eigenvalues, $0 < c < 1$, when $Q_1 = 1$, the left-hand side of (3.13) is small to order c_i. On the right-hand side of (3.13), we note that the contribution of $Im(p^*S_1)$ is of order $(Q_1 - 1) \cdot c_i$ since ϕ is real for $Q_1 = 1$. The other term, $Im(\phi^*S_0)$ in (3.13), or

$$Im \int_0^1 \bar{h}\phi^* V \frac{dQ_1/dz}{z - c}\, dz \tag{3.16}$$

will, as we shall see, be of a larger, $O(c_i)$, magnitude. The main contribution to the integral in (3.16) comes from the critical layer, y_c, where $c_r = z_c = \exp(y_c) = \bar{u}(y_c)$. At this critical layer the x momentum equation (3.1) implies for $Q_1 \approx 1$

$$\bar{h}V = -\phi + O(Q_1 - 1),\ z \to z_c. \tag{3.17}$$

By using this to eliminate V and by taking the principal part of (3.16), we get

$$Im \int_0^1 \bar{h}V\phi^* \frac{dQ_1/dz}{z - c}\, dz \approx - Im \int_{z_c^-}^{z_c^+} |\phi|^2 \frac{dQ_1/dz}{z - c}\, dz \tag{3.18}$$

$$= -|\phi(z_c)|^2 \frac{dQ_1(z_c)}{dz} \cdot \pi \operatorname{sign}(c_i) \tag{3.19}$$

where the calculus of residues has been used to obtain the last results. Equating (3.15) and (3.19) we see that if $c_i \neq 0$, then

$$\frac{dQ_1(z_c)}{dz} > 0, \tag{3.20}$$

i.e. the potential vorticity has to increase *toward* the front for the mode to amplify. We now show that the nondispersive long waves exist for $Q_1 = 1$, and we shall discuss their significance in Section 6.

We substitute $\phi(z)$ from Eq. (3.9) into Eq. (3.10) (with $S_1 = S_0 = 0$) to get a single O.D.E. for $p(z)$. The resulting equation can be written in terms of $q(z) \equiv z\, dp/dz$ as

$$(r - 1 + z)z^2 q_{zzz} + 3z(2z + r - 1)q_{zz} + \left(6z + \frac{z}{c} - 1\right)q_z + \frac{2}{c}q = 0. \tag{3.21}$$

The boundary conditions (3.11a,b) become $q(1) = 0 = q(0)$. The points $z = 0, -(r - 1)$ are regular singular points of equation (3.12), and the solution can be expressed as a Frobenius series

$$q(z) = z^\alpha \sum_{n=0}^{\infty} a_n z^n,\ a_0 \neq 0. \tag{3.22}$$

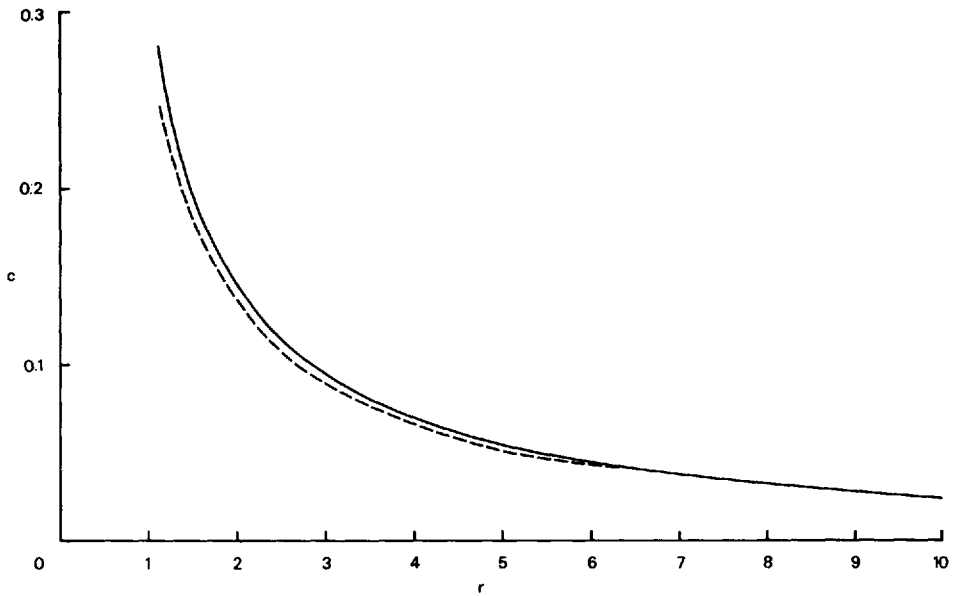

Figure 2. Phase speed c as a function of r for a front of uniform potential vorticity. The firm line shows the exact result, derived by numerical integration and series summation. The dashed line shows the large r asymptote $c \approx 0.272\, r^{-1}$.

When (3.22) is substituted into (3.21), we find that the indicial equation for the index α (by equating to zero the coefficients of $z^{\alpha-1}$) is:

$$\alpha[(r-1)(\alpha^2-1)-1] = 0$$

and the index α which yields a solution which satisfies $q(0) = 0$ is

$$\alpha = \left[\frac{r}{r-1}\right]^{1/2}.$$

By equating to zero the coefficient of $z^{n+\alpha}$, we find the recursion relation for $\{\alpha_n\}$

$$a_{n+1} = -a_n \frac{(n+\alpha-1)(n+\alpha)(n+\alpha+4) + \left(6+\frac{1}{c}\right)(n+\alpha) + \frac{2}{c}}{(r-1)(n+\alpha)((n+\alpha)^2-1) + 3(r-1)} \qquad (3.23)$$
$$(n+\alpha)(n+\alpha+1) - (n+\alpha+1)$$

From (3.23) we see that $|a_{n+1}/a_n| \to (r-1)^{-1}$ as $n \to \infty$ and the series (3.22) will converge at $z = 1$ for $r - 1 > 1$, i.e. when the lower layer is deeper than the upper layer. The divergence for $r - 1 < 1$ is due to the additional singularity at $z = -(r-1)$ of (3.21) and does not impede direct numerical integration of the equation between $z = 0$, 1.

By fixing r we can sweep over the value(s) of c for which the boundary condition $q(1) = 0$ is satisfied. The resulting $c(r)$ for the largest eigenvalue is given in Figure 2.

These values were computed by direct integration of the equation (3.21) and for the $r > 2$ (i.e. $r - 1 > 1$) region were checked against a summation of the Frobenius series (3.22), i.e.

$$q(1) = \sum_{n=0}^{N} a_n = 0.$$

The $r \to \infty$ asymptote of the $c(r)$ curve in Figure 2 can be computed analytically by taking the limit $r \gg h$ in (3.9), viz.

$$r \frac{d}{dz}\left(z \frac{dp}{dz}\right) + \frac{p}{c} = \frac{-\phi}{z}.$$

For $p \approx 0(1)$, the terms balance if $c^{-1} \approx r$, $r \to \infty$ and if ϕ and h are $0(r)$. In this case we define

$$\frac{\lambda^2}{4} = \frac{1}{rc}$$

to obtain

$$\frac{d}{dz}\left(z \frac{dp}{dz}\right) + \frac{\lambda^2}{4} p = \frac{-\phi}{rz}. \tag{3.24}$$

Now, (3.10), (3.12a, b) have to leading order the trivial solution $\phi = Arz$ for some A. Thus, the solution of (3.24) is

$$p(z) = J_0(\lambda z^{1/2}) - \frac{4A}{\lambda^2} \tag{3.25}$$

where J_0 is the Bessel function of the first kind, of order zero. (A is determined from (3.11b) as $\lambda^2/4$.) The boundary condition (3.11a) implies

$$J_1(\lambda) = 0 \tag{3.26}$$

and therefore

$$c_n = \frac{4}{\lambda_n^2} \cdot \frac{1}{r} \tag{3.27}$$

where λ_n is the nth zero of J_1. The asymptote of $c(r)$ in Figure 2 agrees well with the formula

$$c_0 = \frac{4}{\lambda_0^2} \cdot \frac{1}{r} = \frac{0.2724}{r}. \tag{3.27a}$$

We may also derive a relation between the position of the front, (y_f), and a fluctuating transport such as may be imposed at some upstream point (a narrow strait

from which the frontal system emerges, for example). The transport between any two points $y_1 = A$, $y_2 = B$, in the upper and lower layer is

$$M_{AB} = \int_A^B [uh + u_2(r - h)]dy = \int_A^B h(u - u_2)dy + r\int_A^B u_2 dy \qquad (3.28)$$

Since $u = -\phi_y$, $u_2 = -p_y$, $h = \phi - p$, we get from (3.28)

$$M_{AB} = -\frac{1}{2}h^2\Big|_A^B - rp\Big|_A^B \qquad (3.29)$$

If we compute the total transport between $y = -\infty$ and $y = \infty$ (where p is constant) and $h(-\infty) = 1$, $h(\infty) = 0$,

$$M_T = \frac{1}{2}. \qquad (3.30)$$

If, on the other hand, we compute the total transport to the left of the free streamline, i.e. where there is only one layer of fluid, we get

$$M_+ = -\frac{1}{2}h^2\Big|_{y_f}^{\infty} - rp\Big|_{y_f}^{\infty} = rp(y_f) \approx rp(0) \qquad (3.31)$$

where $p(\infty) = 0$ has been used. Therefore, the transport perturbation in this front to the right of y_f (which involve both layers of fluid) $M' = -M_+$ is

$$M' = -rp(0). \qquad (3.32)$$

Now consider the linearized position of the free streamline which can be computed from

$$0 = h(y_f) = h'(0) + \frac{d\bar{h}}{dy}(0) \cdot y_f = h'(0) - \bar{u}(0)y_f$$

so that

$$y_f = \frac{h'(0)}{\bar{u}(0)} = \phi(0) - p(0) \qquad (3.33)$$

for $\bar{u}(0) = 1$. Therefore

$$\frac{y_f}{M'} = \frac{-(\phi(0) - p(0))}{p(0)} \cdot \frac{1}{r} = \frac{1 - \phi(0)/p(0)}{r}. \qquad (3.34)$$

The ratio on the right-hand side of (3.34) can be computed from the asymptotic solutions for ϕ, p as $r \to \infty$ which were derived in (3.24) – (3.26),

$$\frac{\phi(0)}{p(0)} \approx \frac{\frac{\lambda_0^2}{4} r}{J_0(\lambda_0) - 1}$$

where λ_0 is the first zero of J_1. Therefore (3.34) becomes to order r^{-1}

$$\frac{y_f}{M'} \approx \frac{\lambda_0^2/4}{1 - J_0(\lambda_0)} \approx 2.6 \tag{3.35}$$

and the numerical solutions show this asymptotic to hold for $r \geq 2$.

4. More general instability considerations

The foregoing analysis pertains only to one type of long wave, which amplifies only under very special circumstances, and we shall show that there are other dispersive modes which amplify even when $Q_1 = 1$. The important general conclusion will be reached that all fronts are unstable to long waves, subject only to a formal restriction that the lower layer be sufficiently deep. Other considerations indicate that the shallower the lower layer, the more rapid the instability.

The following asymptotic analysis is not only based on a small wavelength (ϵ) expansion of (2.18) to (2.21) but also on a large depth (r) value, i.e. let

$$r = \frac{K}{\epsilon}, \epsilon \to 0 \tag{4.1}$$

where K is an arbitrary constant of order unity. The restriction to large values of r represents a natural extension of earlier one-layer ($r = \infty$) models, but the reason for choosing the ϵ^{-1} dependence (4.1) is not obvious; we were led to this by prior numerical experimentation. Be this as it may the reader can convince himself that an expansion in ϵ only, with r arbitrary, will fail due to the singularity of Eq. (2.18) as $r \to 1$.

In seeking an expansion of the eigenfunctions in powers of ϵ a problem arises in connection with the lower-layer equation (2.18) at large y. Assuming that $|\bar{u}| \to 0$ faster than $O(|y|^{-2})$ as $y \to -\infty$ (the other cases can also be treated and yield the same answer after rather more algebra), p satisfies

$$p_{yy} = \epsilon^2 p, y \to -\infty \tag{4.2}$$

similar to $y > 0$. This demonstrates the necessity of an outer expansion for which a stretched coordinate $Y = \epsilon y$ is needed, so that (4.2) yields $p \propto \exp(Y)$. This will modify the boundary condition on p for y of order unity; the relevant boundary conditions are derived in the Appendix and are quoted as necessary.

To proceed, we note that for $\epsilon = 0$,

$$h = \bar{u}, u = -\bar{u}_y, V = \bar{u}, p = 0, c = 0 \tag{4.3}$$

is a trivial solution (corresponding to a lateral shift by the front) which satisfies all the boundary conditions. We use this as a basis for an expansion in small ϵ

$$\begin{aligned} h &= \bar{u} + \epsilon h_1 + \epsilon^2 h_2 + \ldots \\ p &= \epsilon p_1 + \epsilon^2 p_2 + \ldots \\ c &= \epsilon c_1 + \epsilon^2 c_2 + \ldots \end{aligned} \tag{4.4}$$

and similarly for $u = -\bar{u}_y + \ldots$ and $V = \bar{u} + \ldots$. The suffices 1 and 2 here should not be confused with the notation for upper and lower layer. Collecting terms $0(\epsilon)$, $0(\epsilon^2)$ for the lower-layer equation (2.18), we get

$$0(\epsilon): Kc_1 p_{1yy} = -\bar{u}(p_1 + c_1) \tag{4.5}$$

$$0(\epsilon^2): Kc_2 p_{1yy} - \bar{h}c_1 p_{1yy} + Kc_1 p_{2yy} = -c_1 h_1 - c_2 \bar{u} - c_1 \bar{u} q_{1y} - \bar{u} q_2 \tag{4.6}$$

with boundary conditions (see Appendix)

$$P_{1y} = 0, \quad y = 0 \tag{4.7}$$

$$p_{2y} = -p_1, \; y = 0 \tag{4.8}$$

$$p_1 \longrightarrow \text{constant}, \; y \longrightarrow \infty \tag{4.9}$$

$$p_{2y} \longrightarrow \quad p_1, \quad y \longrightarrow -\infty. \tag{4.10}$$

Note that to leading order there is no interaction with the upper layer. A trivial solution of (4.5) is

$$p_1 = -c_1. \tag{4.11}$$

(There are other solutions in general, but these have c_1 determined at this order so that the subsequent solvability condition (4.23) is not satisfied.)

To solve the top-layer equations to order $\epsilon^i (i = 1, 2, \ldots)$, we write them symbolically

$$\bar{u} u_i + (1 - \bar{u}_y) V_i + \phi_i = A_i \tag{4.12}$$

$$\bar{u} + \phi_{iy} = B_i \tag{4.13}$$

$$\bar{h} u_i - (\bar{h} V_i) y + \bar{u} h_i = C_i \tag{4.14}$$

where A_i, B_i, C_i represent known functions of order $\epsilon^0, \epsilon^1, \ldots \epsilon^{i-1}$, which will have been evaluated already in the preceding step. (None are present for $i = 0$.) We write

$$u_i = B_i - \phi_{iy} \tag{4.15}$$

and substitute into (4.12) for V_i:

$$V_i = \frac{A_i - \phi_i - \bar{u} B_i + \bar{u} \phi_{iy}}{1 - \bar{u}_y} \tag{4.16}$$

and use both expressions in (4.14) to give

$$\bar{h}B_i - \bar{h}(p_{iy} + h_{iy}) - \left\{\frac{\bar{h}}{1-\bar{u}_y}(A_i - \phi_i - \bar{u}B_i + \bar{u}\phi_{iy})\right\}_y + \bar{u}h_i = C_i. \tag{4.17}$$

Noting the terms in h_i are a perfect differential, we may integrate from 0 to y and use the well-behaved condition to give, after multiplication by $(1 - \bar{u}_y)\bar{h}^{-1}$, and integration by parts on $\bar{h}p_{iy}$,

$$\bar{u}\phi_{iy} - \bar{u}_y\phi_i = \bar{u}B_i - A_i - \left[\frac{1-\bar{u}_y}{\bar{h}}\right]\int_0^y (C_i - \bar{h}B_i - \bar{u}p_i)dy. \tag{4.18}$$

Note that p_i occurs on both sides of (4.18).

To $0(\epsilon)$, we have $A_1 = c_1\bar{u}_y$, $B_1 = 0$, $C_1 = c_1\bar{u}$ which together with (4.11) and a little algebra, reduces to

$$\bar{u}h_{1y} - \bar{u}_y h_1 = 0 \tag{4.19}$$

so that $h_1 \propto \bar{u}$. By choosing the amplitude of h to be $\bar{u}(0)$, we have

$$h_1 \equiv 0. \tag{4.20}$$

This is to be expected, as the first ageostrophic terms do not enter in (2.20) until order ϵ^2, and the geostrophic part of the solution is already contained in (4.3). The solution (4.20) simplifies the lower-layer equation (4.6), which yields

$$Kc_1 p_{2yy} = -\bar{u}(p_2 + c_2) \tag{4.21}$$

together with conditions (4.8), (4.10). Fortunately it is not necessary to solve this equation to proceed.

To obtain c_1, we examine the top layer at $0(\epsilon^2)$. Following the previous procedures gives

$$A_2 = -c_2\bar{u}_y,\ B_2 = \bar{u}^2,\ C_2 = c_2\bar{u},$$

so that after substitution in (4.18),

$$\bar{u}\phi_{2y} - \bar{u}_y\phi_2 = \bar{u}^3 + c_2\bar{u}_y - \left[\frac{1-\bar{u}_y}{\bar{h}}\right]\int_0^y (c_2\bar{u} - h\bar{u}^2 - \bar{u}p_2)dy. \tag{4.22}$$

The first term in the integrand is an exact differential, by (4.5). In the third term, we note that $\bar{u}p_2$ also appears in (4.21), so that (4.22) becomes, after integration of (4.21) and use of (4.8),

$$\bar{u}\phi_{2y} - \bar{u}_y\phi_2 = \bar{u}^3 + c_2\bar{u}_y + \frac{1-\bar{u}_y}{\bar{h}}\int_0^y \bar{h}\bar{u}^2 dy + Kc_1\left[\frac{1-\bar{u}_y}{\bar{h}}\right][p_{2y} - c_1] \tag{4.23}$$

where the very last term comes from the boundary condition on $y = 0$.

There is no need to solve this equation either, since the solvability condition will determine c_1. For large values of y (but $\epsilon \mid y \mid$ still small), ϕ_2 and $\bar{u}$ tend to zero and $p_{2y} \rightarrow \bar{p}_1 = -c_1$ from (4.10), so that the sole surviving terms of (4.23) are

$$\int_0^{-\infty} \bar{h}\bar{u}^2 dy - 2Kc_1^2$$

which must vanish in order for (4.23) to have solutions bounded at infinity. Hence

$$c_1^2 = \frac{-1}{2K} \int_{-\infty}^{0} \bar{h}\bar{u}^2 dy \tag{4.24}$$

which is clearly negative, so that

$$c_1 = \pm i \left[\frac{\int_{-\infty}^{0} \bar{h}\bar{u}^2 dy}{2K} \right]^{1/2} \tag{4.25}$$

or, using (4.1) to revert to r rather than k,

$$c \approx \pm i \left[\frac{\epsilon \int_{-\infty}^{0} \bar{h}\bar{u}^2 \, dy}{2r} \right]^{1/2}, \epsilon \rightarrow 0, r \text{ not too small}, \tag{4.26}$$

which is the fundamental result of this section. The positive root of (4.26) shows that all isolated fronts (as we have defined them) are unstable, no matter what their shape or potential vorticity distribution. In this connection we note that the lower-layer potential vorticity is $(r - \bar{h})^{-1}$, normally a monotonically decreasing function of y, and the undisturbed structure of the upper layer may easily be chosen so as to have potential vorticity also decreasing with y. The above results show that even this state is unstable and that a change in sign of potential vorticity gradient is not a requirement for instability when a front exists.

Since the mean state (denoted by a bar) contains kinetic as well as available potential energy, the important question arises as to the sense of the transfer of each of these terms to the perturbation (again denoted by a prime). To investigate this, one takes the perturbation equations formed from (2.1), (2.2), (2.3), multiplies them by $\bar{h}u'$, $\bar{h}v'$, h' respectively and adds the results for the two layers. With angle brackets denoting a x average, and with numerical suffices now referring to the layer number, we find that an expression for the total perturbation energy E satisfies

$$\frac{\partial E}{\partial t} + \bar{h}\bar{u}_y \langle u'_1 v'_1 \rangle + \bar{u} \langle h'_x p' \rangle + \frac{\partial}{\partial y} \left\{ \langle \bar{h} v'_1 (h' + p') + (r - \bar{h}) v'_2 p' \rangle \right\} = 0, \tag{4.27}$$

$$E = \left\langle \bar{h} \left(\frac{1}{2} u'^2_1 + \frac{1}{2} \epsilon^2 v'^2_1 \right) + \frac{1}{2} h'^2 + (r - \bar{h}) \left(\frac{1}{2} u'^2_2 + \frac{1}{2} \epsilon^2 v'^2_2 \right) \right\rangle. \tag{4.28}$$

Integration over y then gives

$$\frac{d}{dt}\int_{-\infty}^{0} E\,dy + \int_{-\infty}^{0} \bar{h}\bar{u}_y \langle u'_1 v'_1 \rangle\,dy + \int_{-\infty}^{0} \bar{u}\,\langle h'_x p' \rangle\,dy = 0, \tag{4.29}$$

showing that energy changes are effected by the Reynolds stress term in the upper layer, and the term depending on the phase difference between upper and lower-layer pressure (NB. $\langle h'_x p' \rangle = \langle \phi'_x p' \rangle$). In GKS, KS, and Killworth (1983), only the Reynolds stress term appeared, as the lower layer was assumed infinitely deep at rest. Now the possibility of vertical interactions permits true baroclinic effects between layers.

We have, from the current work,

$$\begin{aligned} u_1 &\approx -\bar{u}_y + 0(\epsilon^2) \\ V_1 &\approx -\bar{u} + \epsilon c_1 + 0(\epsilon^2) \\ h &\approx \bar{u} + 0(\epsilon^2) \\ p &\approx \epsilon c_1 + 0(\epsilon^2), \end{aligned} \tag{4.30}$$

so that the Reynolds stress is given by

$$\langle u'_1 v'_1 \rangle = -\tfrac{1}{2}\, Im(uV^*) = \frac{-\epsilon \bar{u}_y}{2}\, Im(c_1), \tag{4.31}$$

where stars denote complex conjugates. This result is identical to those in the one-layer papers. The vertical baroclinic term is given by

$$\langle h'_x p' \rangle = \tfrac{1}{2}\, Re(i\, h\, p^*) = \frac{-\epsilon \bar{u}}{2}\, Im(c_1), \tag{4.32}$$

and by inserting these into (4.29), we have the neat result

$$\frac{d}{dt}\int_{-\infty}^{0} E\,dy = \frac{\epsilon\, Im(c_1)}{2}\left\{\int_{-\infty}^{0} \bar{h}\bar{u}_y^2 dy + \int_{-\infty}^{0} \bar{u}^2\,dy\right\}. \tag{4.33}$$

For wide currents, the second (baroclinic) term dominates; for narrow currents, the first (barotropic) term is dominant. In general, then, the instability is *mixed*, in that both energy production mechanisms contribute to the instability.

As in Section 3, a convenient amplitude measure is the ratio of frontal displacement y_f to the perturbation mass flux, the latter being again defined as

$$M' = \int_{-\infty}^{0} \{\bar{h}u_1 + \bar{u}h_1 + (r - \bar{h})u_2\}\,dy \tag{4.34}$$

Using (2.14), (2.17), we find after a little simplification

$$M' = irv_2\,|_{y=0} \tag{4.35}$$

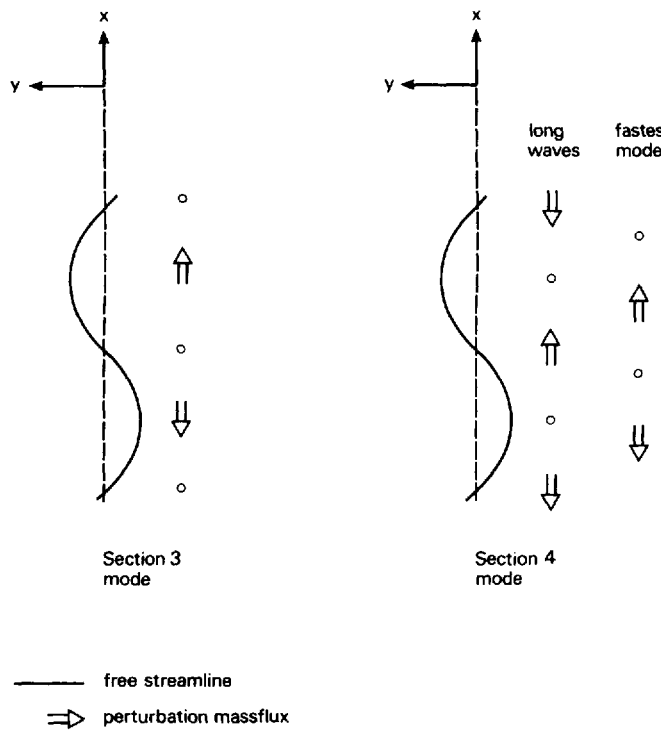

Figure 3. The schematic relationship between the phases of the free streamline derivation and perturbation mass fluxes on the two-layer side of the front (to the right in the diagram), for the modes in Sections 3 and 4. In the latter case, both the long-wave limit and the fastest-growing mode (for uniform potential vorticity) are shown.

But $v_2 = cy_f/i$ at the free streamline ($y \approx 0$) and therefore

$$\frac{y_f}{M'} = \frac{1}{rc} = \frac{-i}{(\epsilon r)^{1/2}}\left[\frac{2}{\int_{-\infty}^{0} \bar{h}\bar{u}^2 dy}\right]^{1/2} = \frac{-0.29i}{(\epsilon r)^{1/2}} \tag{4.36}$$

where the last result applies for uniform potential vorticity.

The waves discussed in Sections 3 and 4 are thus seen to be quite different. The near-uniform potential vorticity instability has a perturbation mass flux in phase with the meanders of the free streamline; the instability in this section has a perturbation transport $\pi/2$ out of phase with the free streamline. Figure 3 shows a schematic of these differences.

5. Numerical confirmation and comparisons

a. Numerical results. The analyses of the previous two sections, which are relevant only for long waves, have been confirmed and extended numerically by direct solutions of (2.12), (2.13), (2.14). Figure 4 shows c_i and ϵc_i for the uniform potential vorticity

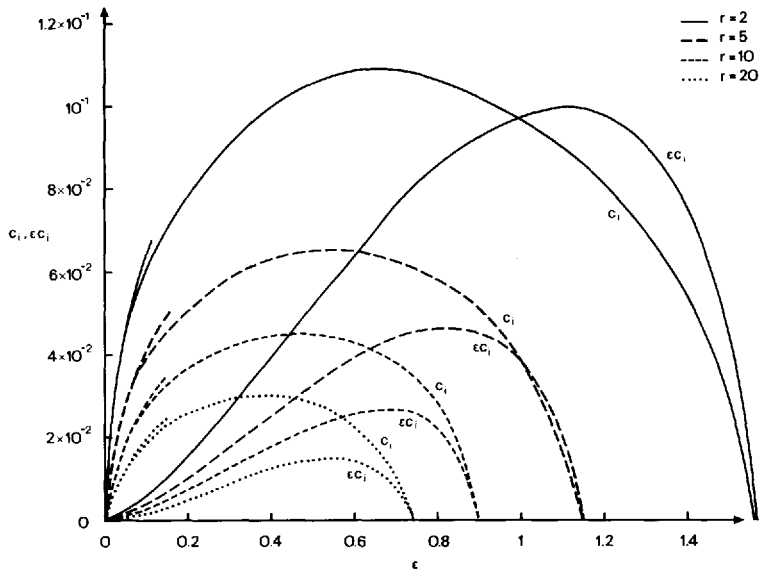

Figure 4. Imaginary parts of c, and growth rates $\epsilon\, c_i$, as a function of wavenumber ϵ, for total depths $r = 2$ (—), 5 (– –), 10 (----) and 20 (. . . .). Also shown, for small ϵ, are the asymptotics of c_i for small ϵ given by (4.26).

mean flows (2.10), (2.11), for varying ϵ and r. The unstable mode of Section 3 (for a suitable mean profile) has been computed, but its growth rate is of order 10^{-5} and so cannot be displayed on the diagram.

For small ϵ, the solution lies very close to the asymptotic value of Section 4; this asymptote is also shown on Figure 4. The error, as predicted, is $0(\epsilon)$, and the asymptote remains excellent even for r as small as 2. (This is shown more clearly in Figure 5 for values of $r = 2$, 5, 10, and 20.) The values of c_r, not shown for reasons of clarity, increase as ϵ for small ϵ, as would be expected from the next term in the expansion. Figure 5 shows that c_r, like c_i, decreases with lower-layer depth, qualitatively like the mode in Section 3.

Solutions for the four values of r all display a high wavenumber cutoff, presumably associated with the uniform potential vorticity used. GKS and KS both found high wavenumber modes confined to the front in one-layer models, and these may well persist in this two-layer model for other mean profiles.

The fastest-growing mode has $c_r \approx c_i$. This alters the ratio of free streamline displacement y_f to perturbation mass flux M', so that $y_f/M' \approx \exp(-i\pi/4)$, as indicated on Figure 3. A phase shift of $\pi/4$ is still likely to be distinguishable from one of zero in observations, however.

b. Comparison with Phillips' (1954) quasi-geostrophic model. Much of this behavior is qualitatively similar to Phillips' (1954) two-layer quasigeostrophic model, as

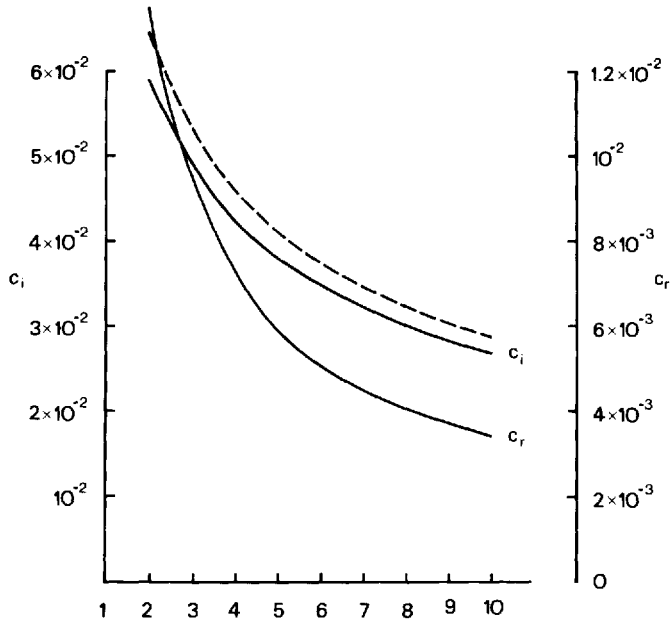

Figure 5. c_r and c_i for $\epsilon = 0.1$, as functions of r; note the different scales. Shown dashed is the asymptotic (4.26) for c_i, whose error is uniformly $0(\epsilon)$.

discussed in Griffiths and Linden (1982). The success of this model was quite surprising, as it badly misrepresented the physics (Rossby numbers of order unity, vanishing layer depths, etc.). It seems worthwhile to compare Phillips' model with our new model to see why it fared so well and where it may break down.

To perform such a comparison, we scale the deformation radius on a mean depth H of the lighter layer, apply a uniform mean flow in that layer of $(g'H)^{1/2}$, (far beyond the permissible limits of quasigeostrophy), and apply no mean flow in the lower layer. For perturbations varying as $\exp i\, k(x - ct)$, where k is scaled on the deformation radius, the Phillips model for a flow unbounded in y gives

$$c = \frac{1}{2(1 + k^2 + \delta)} \left\{ 2\delta + k^2 \pm \sqrt{(k^4 - 4\delta)} \right\} \tag{5.1}$$

where δ is the ratio of layer depths $(r - 1)^{-1}$. As this becomes small, we must have $k = \alpha\delta^{1/4}$ for instability, where α is of order unity. This yields

$$c \approx \frac{(r - 1)^{1/2}}{2} \left\{ \alpha \pm i\sqrt{(4 - \alpha^4)} \right\}, \quad r \to \infty \tag{5.2}$$

so that c_r, c_i are both $0(\delta^{1/2})$, and the growth rate

$$kc_i = \frac{1}{2}(r-1)^{-3/4}\,\alpha\sqrt{(4-\alpha^4)}. \tag{5.3}$$

This has a high wavenumber cutoff for

$$k_{\text{cut}} = 2^{1/2}(r-1)^{-1/4} \tag{5.4}$$

and maximum growth at

$$k_{\max} = \left(\frac{4}{3}\right)^{1/4}(r-1)^{-1/4} \tag{5.5}$$

which is

$$(k\,c_i)_{\max} = 0.88\,(r-1)^{-3/4}. \tag{5.6}$$

These predictions may be compared with the uniform potential vorticity solutions in Figures 4 and 5, as summarized in Figure 6 (some points are approximate due to numerical errors). The high wavenumber cutoff here appears to vary as $(r-1)^{-1/4}$, but with a coefficient of order 1.6, a little higher than the Phillips prediction of 1.4. However, the wavenumber of maximum growth varies as $1.15\,(r-1)^{-1/4}$, which is in excellent agreement with the 1.08 predicted quasigeostrophically.

The main disagreement occurs for the growth rate $(\epsilon c_i)_{\max}$. The scatter in Figure 6 is a little higher than for ϵ alone, but a fit of $0.13\,(r-1)^{-3/4}$ is not too bad. This value is almost seven times smaller than the Phillips' model yields, but this discrepancy could probably be reduced by introducing rigid y-boundaries to simulate the natural frontal confinement.

c. Comparison with experiments. The foregoing remarks may rationalize the surprising success of the Phillips (1954) model as applied to laboratory results by Griffiths and Linden (1982). For fronts sufficiently far from any boundaries, they found experimentally that (in our notation) the wavelength of the fastest-growing mode scaled with $\delta^{1/4}$ (i.e. scales on the geometric mean of the deformation radii of the two layers) and that $\delta^{1/4}\epsilon \approx 1.1 \pm 0.3$ which was consistent with the Phillips' result of 1.08 mentioned above. It is also, of course, consistent with the 1.15 figure found in this paper, although this prediction of wavelength seems a little small for Griffiths' and Linden's isolated vortex instability (their Fig. 10). There is also excellent agreement with the figure of 1.16 ± 0.27 found by Chia *et al.* (1982).

We also note that our model predicts rather small values of c_r even when r becomes quite close to two, in good agreement with the experimental results which show almost stationary perturbations (until nonlinear amplitudes are attained). For the case in Griffiths' and Linden's Figure 11 (an isolated vortex), the Phillips' model predicts $c_r \approx$

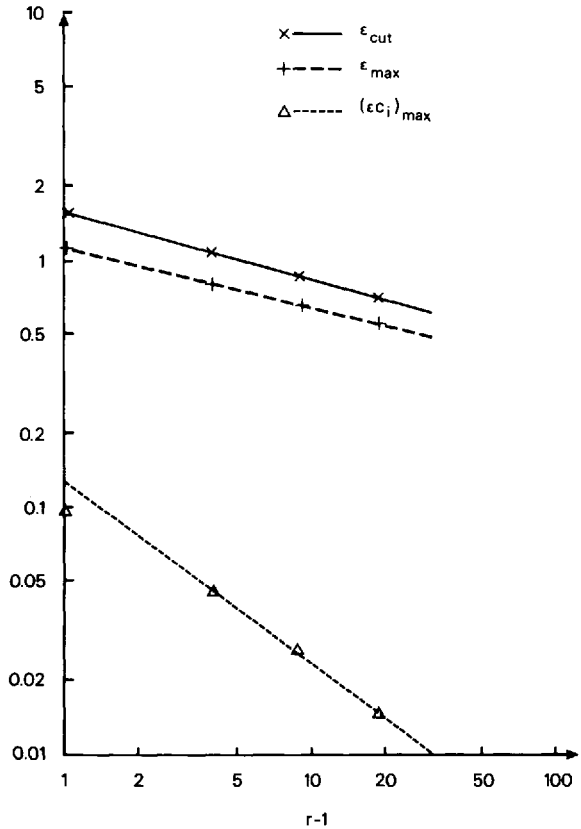

Figure 6. The approximate values of the cutoff wavenumber ϵ_{cut}, the wavenumber of maximum growth ϵ_{max}, and the maximum growth rate $(\epsilon\, c_i)_{max}$, for values of $r = 2$, 5, 10 and 20 and uniform potential vorticity. The three power laws, fitted by eye, are, reading downward, $1.6\,(r-1)^{-1/4}$, $1.15\,(r-1)^{-1/4}$, $0.31\,(r-1)^{-3/4}$.

0.66, whereas our model yields $c_r < 0.1$, an order of magnitude less. (However, the geostrophic adjustment of two finite-depth layers in the Griffiths and Linden experiment would produce a finite counterflow in the lower layer, so that the assumption of our model having no mean flow in the lower layer would be questionable, and the comparison is less than straightforward.)

Similarly, the overestimate of growth rate by the Phillips model yields it less relevant for frontal simulations. For the same isolated vortex, the Phillips model predicts a growth rate of 0.27 (growth by a factor of 30 in one rotation period) compared with the model's prediction of order 0.1 (growth by 3.5 in one rotation period). Estimates of growth rates from experiment are notoriously difficult to make, but Griffiths' and Linden's Figure 11 would tend to support the lower of these values rather than the higher.

d. Comparison with oceanic observations. Application of a linear idealized model to the complicated nonlinear dynamics of the real ocean is a more difficult task. Killworth (1983) compared a one-layer frontal model with the Gulf Stream observations summarized by Fofonoff (1981) and found reasonable agreement for predicted wavelength and period, but far too small a predicted growth rate.

We may also examine the results of the two-layer model. Take $f \approx 10^{-4}\text{s}^{-1}$, deformation radius $a \approx 30$ km, and H to be a typical depth of the 15° isotherm, say 600 m. With a depth of 4000 m, this gives $r \approx 7$. The predictions from Figure 6 give, for the fastest-growing wave, $\epsilon \approx 0.7$, $c_i \approx c_r \approx 0.043$. This translates dimensionally to a wavelength of 270 km, while Fofonoff quotes 140–365 km. This wide range, presumably caused by slope and shelf effects, means that any prediction with a wave length of order 2π deformation radii would give reasonable agreement.

The prediction for frequency is $f(\epsilon c_r)$, giving a period of $2\pi(f\epsilon c_r)^{-1} \approx 24$ days; Fofonoff cites 10 to 37 days, so again the prediction is in the right range. Growth rates are predicted to be of order $f(\epsilon c_i) \approx 0.25$ days^{-1}, perhaps a little rapid compared with the observed values of 0 to 0.2 days^{-1} quoted. Finally, the phase speed is $fa(c_r) \approx$ 13 cm s^{-1}, which lies within the observed 9 to 17 cm s^{-1}, with smaller values over the deeper ocean. The wide spread of observed values means that all one can say is that predicted wave parameters are in about the right range.

We have not attempted comparisons with shelf-slope observations (cf. Lee and Atkinson, 1983), since the influence of bottom topography is clearly important, and may lead to complete stabilization.

6. Discussion

This paper has demonstrated that two-layer fronts with the lower layer at rest in the mean are always unstable to small perturbations. These perturbations have been constructed analytically for long downstream wavelengths, and continued numerically for smaller wavelengths. Two types have been found, the first a weak but nondispersive long-wave instability, the second a strong but dispersive instability. The latter has fastest growth for wavelengths of order the deformation radius, and is of a mixed barotropic-baroclinic nature. The findings about this instability agree well with the experimental findings of Griffiths and Linden (1982). The results are clearly relevant to strong frontal systems like the Gulf Stream, even though the model needs augmentation in various ways.

The theory developed at the end of Section 3 may be relevant to two oceanographic puzzles: the curious seasonal behavior of the flow through the Florida Strait, and the annual cycle of the Loop Current in the Gulf of Mexico.

First, observations of the transport of the Florida current show that it reaches its maximum in June (Niiler and Richardson, 1973). The Sverdrup transport in the North Atlantic subtropical gyre, which should be equal and opposite according to simple

theory, has a marked peak in February (Evenson and Veronis, 1975; Leetmaa and Bunker, 1978). Anderson and Corry (1983) have suggested that topography in the subtropical gyre allows the interaction of barotropic and baroclinic waves producing coastal Kelvin waves. Their results show much better agreement in phase between predicted and observed signals than flat-bottom theory suggests.

Second, Maul (1977) showed how the flow of the Loop Current from the Yucatan to the Florida Straits takes the shortest path during autumn and early winter. It is then deflected continuously northward, increasing the length of its path and the depth of water over which the path lies.

A possible explanation linking the phase lag and the deflection of the Loop Current uses the nondispersive theory in Section 3. In the winter, the subtropical Sverdrup transport is increasing, reaching a maximum in February. This deflects the Loop Current northward: Eq. (3.35) gives the required relation. Thus the path length is increased, and the path is forced to pass over deeper water because of the shelf slope. From Figure 2, this depth increase decreases the phase speed c. The combination of longer path and slower speed can easily account for a tenfold increase in travel time of the transport signal, which in turn will affect the flow in the Florida Strait. Maul's (1977; Fig. 4) data strongly support this suggestion, which is also not in disagreement with Anderson and Corry's (1983) results.

Acknowledgments. Much of this work was performed while the authors were participating in the 1983 Woods Hole Geophysical Fluid Dynamics Summer School; we would like to thank all those involved in making it possible.

APPENDIX

The outer solution

Writing $Y = \epsilon y$ in (4.2) gives

$$p_{YY} = p \tag{A1}$$

for very large $| Y |$. The expansion (4.4) then gives

$$p_1 = \alpha e^Y \tag{A2}$$

$$p_2 = \beta e^Y \tag{A3}$$

for some constants α, β, which are to be matched to the inner layer where $y = 0(1)$. To leading order,

$$p_1 \text{ (inner)} \to \alpha, \ | y | \to \infty \tag{A4}$$

so that p_1 becomes a constant for large $| y |$. To next order, the outer p resembles

$$p \approx \epsilon p_1 + \epsilon^2 p_2 \approx \epsilon \alpha (1 + Y) + \epsilon^2 \beta \tag{A5}$$

for small $| Y |$. Hence the inner p must behave as

$$p \approx \epsilon p_1 + \epsilon^2 p_2 \approx \epsilon \alpha + \epsilon^2 (\alpha y + \beta), \ | y | \to \infty. \tag{A6}$$

So the condition on p_2 is

$$p_2 \text{ (inner)} \longrightarrow yp_1 + \beta, \mid y \mid \longrightarrow \infty. \tag{A7}$$

REFERENCES

Anderson, D. L. T. and R. A. Corry. 1983. Ocean response to low frequence wind forcing with applications to the seasonal variation in the Florida Straits. Prog. in Oceanog., (in press.)

Chia, F., R. W. Griffiths and P. F. Linden. 1982. Laboratory experiments in fronts. Part II. The formation of cyclonic eddies at upwelling fronts. Geophys. Astrophys. Fluid Dyn., *19,* 189–206.

Evenson, A. J. and G. Veronis. 1975. Continuous representation of wind stress and wind stress curl over the world ocean. J. Mar. Res., *33,* (Suppl.), 131–144.

Fofonoff, N. P. 1981. The Gulf Stream system, *in* Evolution of Physical Oceanography, B. A. Warren and C. Wunsch, eds., MIT Press, Cambridge, MA, 112–139.

Griffiths, R. W., P. D. Killworth and M. E. Stern. 1981. Ageostrophic instability of ocean currents. J. Fluid Mech., *117,* 343–377.

Griffiths, R. W. and P. F. Linden. 1982. Laboratory experiments on fronts. Part I. Density-driven boundary currents. Geophys. Astrophys. Fluid Dyn., *19,* 159–187.

Hoskins, B. J. 1982. The mathematical theory of frontogenesis. Ann. Rev. Fluid Mech., *14,* 131–151.

Joyce, T. M. 1980. On production and dissipation of thermal variance in the ocean. J. Phys. Oceanogr., *10,* 460–463.

Killworth, P. D. 1983. Long-wave instability of an isolated front. Geophys. Astrophys. Fluid Dyn., *24,* 235–258.

Killworth, P. D. and M. E. Stern. 1982. Instabilities on density-driven boundary currents and fronts. Geophys. Astrophys. Fluid Dyn., *23,* 1–28.

Lee, T. N. and L. P. Atkinson. 1983. Low-frequency current and temperature variability from Gulf Stream frontal eddies and atmospheric forcing along the southeast U.S. outer continental front. J. Geophys. Res., *88,* 4541–4567.

Leetmaa, A. and A. F. Bunker. 1978. Updated charts of the mean annual wind stress, convergences in the Ekman layers, and Sverdrup transports in the North Atlantic. J. Mar. Res., *36,* 311–322.

Legeckis, R. 1978. A survey of worldwide sea-surface temperature fronts detected by environmental satellites. J. Geophys. Res., *832,* 4501–4522.

Maul, G. A. 1977. The annual cycle of the Gulf Loop Current. Part I: Observations during a one year time series. J. Mar. Res., *35,* 29–47.

Niiler, P. P. and W. S. Richardson, Jr. 1973. Seasonal variability of the Florida Current. J. Mar. Res., *31,* 144–167.

Orlanski, I. 1968. Instability of frontal waves. J. Atmos. Sci., *25,* 178–200.

Paldor, N. 1983. Linear stability and stable modes of geostrophic modes. Geophys. Astrophys. Fluid Dyn., *24,* 299–326.

Pedlosky, J. 1979. Geophysics Fluid Dynamics. Springer-Verlag, New York, 624 pp.

Phillips, N. A. 1954. Energy transformations and meridional circulations associated with simple baroclinic waves in a two level quasi-geostrophic model. Tellus, *6,* 273–286.

Stern, M. E., J. A. Whitehead and B.-L. Hua. 1982. The intrusion of a density current along the coast of a rotating fluid. J. Fluid Mech., *123,* 237–265.

Received: *10 January, 1984;* revised: *11 May, 1984.*